First-principles study on energetics of intrinsic point defects in $LaAlO_3$

Xin Luo,[1,2] Biao Wang,[1,*] and Yue Zheng[1,2]

[1]*State and Key Laboratory of Optoelectronic Materials and Technologies, Institute of Optoelectronic and Functional Composite Materials and School of Physics and Engineering, Sun Yat-sen University, 510275 Guangzhou, China*

[2]*Department of Electronic and Information Engineering, The Hong Kong Polytechnic University, Hong Kong, SAR, China*

(Received 19 March 2009; revised manuscript received 10 June 2009; published 24 September 2009)

Using density-functional theory (DFT) calculations, the formation energies, electron affinities and electronic levels of various intrinsic defects in bulk $LaAlO_3$ are investigated. Results give the atomic structures of charged interstitials, vacancies, Frenkel pairs, antisite defects, and Schottky defects, respectively. It is found that the formation energies of O vacancy are the lowest in the reducing conditions. In contrast, the La vacancy V_{La} is more favorable in formation energy as the O chemical potential increasing. Moreover, by considering the defect levels of $LaAlO_3$ with respect to the silicon conduction bands, the effects of the electron and hole trapping in real devices are also simulated. Our results show that the paired charged V_O, which lies in the middle of the silicon band gap, should be the key problematic defect. The deep defect level of V_O can induce a large-tunneling-leakage current and cause instability in the device performance. These predictions provide rich defect structures in $LaAlO_3$ and useful information for the microelectronic designs.

DOI: 10.1103/PhysRevB.80.104115 PACS number(s): 61.72.J−, 71.15.Mb, 77.84.−s

I. INTRODUCTION

Research on $LaAlO_3$ is experiencing a rapid surge of interest due to its potential use in applications such as high-K gate dielectric.[1] The continued downscaling of Si complementary metal-oxide-semiconductor (CMOS) devices requires the use of a gate dielectric with a high-dielectric permittivity (high K). The high-K materials with larger thickness can avoid the large-tunneling-leakage current, which is a formidable challenge as the traditional SiO_2 approaches its physical limit.[2] Among the many candidates, ZrO_2 and HfO_2 have been highlighted and practically used in the latest techniques, but their crystallization temperature is low (e.g., 400–500 °C). $LaAlO_3$ is a promising gate dielectric material in future CMOS devices due to its large band gap (5.6–6.5 eV) (Refs. 3 and 4) and permittivity $(23-25\varepsilon_0)$.[5,6] It also has good thermodynamic stability in contact with the Si substrates. Crystalline $LaAlO_3$ (100), which is well matched with Si(100) in lattice with a 45 °C rotation, can grow epitaxially on a Si substrate. Moreover, epitaxial Si films maintain an abrupt interface with the $LaAlO_3$ substrate even after annealing at 900 °C.[7]

Recently, amorphous $LaAlO_3$ gate oxides with an effective oxide thickness of 3 Å have been achieved.[8] However, the $LaAlO_3$ film grown on Si is still amorphous. One of the major problems of the amorphous thin film is the high-defect concentration, which will result in charge trapping and cause degradation of Si carrier mobility. Nowadays, the development trends for high-K gate dielectric are the epitaxial growth, which can grow a crystalline film and reduce the defect concentration. Thus facilitate the band-structure tailoring of the artificial material of human interest. Therefore it is worthwhile to investigate the impact of defect on the electronic structure of crystalline $LaAlO_3$. Electron and hole trapping induced by defects may change the electronic structure in the band gap and affect the leakage current. It is well known that the electrical properties of $LaAlO_3$ will vary with different doping type, surface termination, and thermal treatment conditions. For example, at low O partial pressure, the O vacancies at the interface of $LaAlO_3/SrTiO_3$ play an important role in the anomalous conductivity.[9,10] These results indicate that the electrical properties of $LaAlO_3$ affected by the intrinsic defects are very sensitive to the chemical environment of the whole system.

The importance of $LaAlO_3$ for semiconductor devices, where the alignment of various defect levels with the Si conduction-band edges affects the electrical properties, motivates the study on the energetics of intrinsic defects. Previous theoretical studies of $LaAlO_3$ were focus on the structural and surface properties.[11,12] Concerning the defect structure, only the influence of O related defects and the antisites were considered by Xiong *et al.* recently.[13] Their studies, however, did not discuss how the dependence of defect formation energy depends on the O partial pressure. Many other defects, such as cation vacancies, interstitials, and Frenkel defects, etc., have not been investigated. Therefore, without a detail consideration of the various defect structures, it cannot be concluded that which type of defect species is energetically favorable and stable.

In the present work, we will focus on the influence of a variety of neutral and charged defects on the electronic structure of crystalline bulk $LaAlO_3$ by using first-principles plane-wave-based pseudopotential calculations. The formation energies of various defects in the cubic phase of $LaAlO_3$ are comprehensively investigated. The intrinsic defects include vacancies, interstitials, antisites, Frenkel pairs, and partial and full Schottky defects. As stated above, the stable defect states depend on the chemical environment (oxidizing or reducing atmosphere) and therefore the formation energy is computed as a function of the oxygen chemical potential. Taking into account the effect of electrons transferring from (to) the silicon substrate on the charge defect states in $LaAlO_3$, we also calculate the electron and hole affinities of these defects. Their influences on the silicon band gap are also discussed.

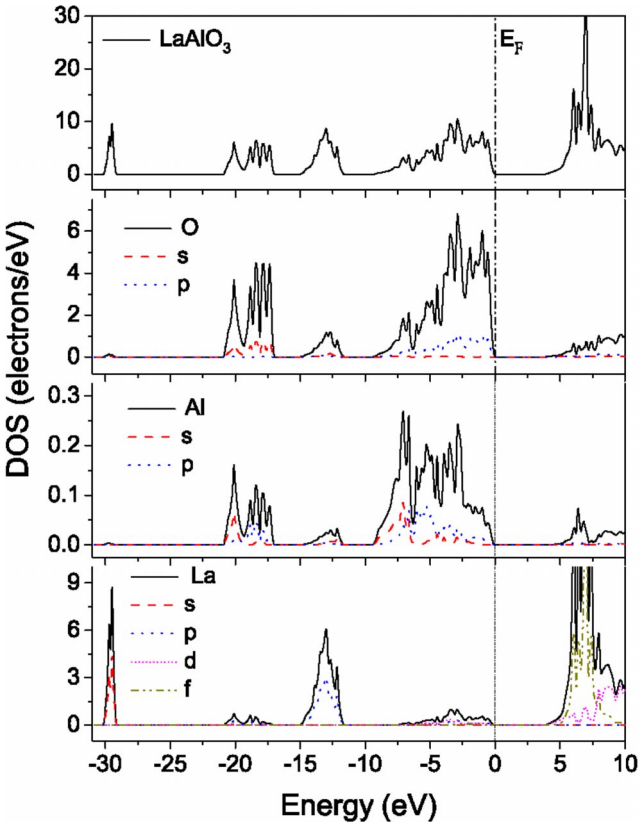

FIG. 1. (Color online) The calculated DOS for $LaAlO_3$.

II. COMPUTATIONAL METHODOLOGY

A. Calculations for perfect structure and supercells

Density-functional theory (DFT) electronic-structure calculations for the structural and electronic properties of $LaAlO_3$ were performed using the Vienna *ab initio* simulation package (VASP).[14] A plane-wave basis set was used for the electronic wave function and the projector augmented wave (PAW) method within the Perdew-Burke-Ernzerhof (PBE) flavor of generalized gradient approximation (GGA) (Refs. 15–17) was used for La, Al, and O atoms. For O, 2*s* and 2*p* electrons were considered as valence electrons while 3*s* and 3*p* electrons were treated as valence electrons in the Al pseudopotential. The PAW pseudopotential of La has 11 valence electrons ($4f$ $5s$ $5p$ $5d$ $6s$). Before going to the supercell calculation of defect structures, test calculations were performed using the PAW pseudopotential for the perfect $LaAlO_3$. For the test calculations, a $6\times6\times6$ mesh was sampled in the irreducible Brillouin zone according to the Monkhorst-Pack method.

The density of states (DOS) of $LaAlO_3$ calculated using GGA is given in Fig. 1. The highest occupied valence band exhibits mainly O $2p$ states whereas the lowest unoccupied conduction band mainly consists of La $4f$ and $5d$ states. The calculated DOS is also consistent with calculations performed by others using the local-density approximation (LDA) calculation.[18] The band-gap value of 3.8 eV calculated by the GGA is 31% less than the experimental value.[3] Since the LDA calculation is well known to underestimate the band gap, the many-body "GW" quasiparticle approximation implemented in the package ABINIT (Ref. 19) was used to correct the band-gap value. In the GW approximation, the ABINIT code used the Kohn Sham electronic structure to compute the screening and the self-energy matrix element at the given k point. $A6\times6\times6$ k mesh with cutoff energy E_{cut}=490 eV is found to be convergent for the Kohn-Sham electronic structure calculation and the converged cutoff energy of the wave function for screening and self-energy calculation are 108 and 135 eV, respectively. The $LaAlO_3$ is a direct band-gap insulator, whose highest occupied and lowest empty bands are located at Γ point.[20] The band gap calculated by the GW method at Γ point is 5.68 eV, which is smaller than the measured value of amorphous $LaAlO_3$ films (6.2 eV),[21] but agrees well with the experimental value of 5.6 eV in crystalline $LaAlO_3$.[3] Table I shows the calculated results of lattice constant, bulk modulus, and the band gap for the cubic type of $LaAlO_3$. These results are compared with the corresponding experiments and other references.[22,23] The optimized lattice constant reproduce well the experimental result, the bulk modulus was obtained by fitting the energy-volume results with a Birch-Murnaghan equation of state. Our results of lattice parameter and bulk modulus are also in good agreement with previous DFT calculations.[18,24]

TABLE I. Calculated and experimental lattice parameters, bulk modulus (B_0), and band gap of the perfect $LaAlO_3$, and are compared with references.

	Lattice constant (Å)	Bulk modulus (GPa)	Band gap (eV)
This work	3.807	194.022	5.677
Experiment	3.829[a]	192.37[b]	5.6[c],6.2[d]
LDA	3.760[e]	217[e]	3.3[e]

[a]Reference 22.
[b]Reference 23.
[c]Reference 3.
[d]Reference 21.
[e]Reference 18.

Based on the optimized test structure, the defect model was simulated with a supercell generated by a repetition of the perfect $LaAlO_3$ in the X, Y, and Z directions. The point defects were introduced by adding and removing atoms for interstitials and vacancies, respectively. The Frenkel defects were introduced by generating a nearby pair of vacancies and interstitials. The Schottky defects were generated by combining various vacancies ($2V_{Al}^{3-}+3V_{O}^{2+}$, $2V_{La}^{3-}+3V_{O}^{2+}$ and $V_{Al}^{3-}+V_{La}^{3-}+3V_{O}^{2+}$). Since the La and Al have the same valence charge, the Al and La antisite defects were also considered. The Al antisite defect Al_{La} occurs when the occupation of a La site in the lattice is replaced by an Al atom and the La antisite defect La_{Al} is the counterpart of the Al-antisite defect. Besides the neutral defects, we also considered various charged defects. The charges were controlled by the total number of electrons in the supercell. When the net charge of the unit cell deviates from zero, a uniform compensating background mirror charge[25] can be incorporated to avoid the divergence of the Coulomb energy. An alternative method to

minimize the effects of the spurious interactions between the defects and their mirror images is using large supercells. To achieve that, we used different supercell sizes, such as $1\times2\times2$, $2\times2\times2$, $2\times3\times3$, and $3\times3\times3$ to analyze the system-size convergence. All supercells were fully relaxed, where for the calculation of the lattice relaxation, the atoms were allowed to move until the residual forces of atoms were less than 0.01 eV/Å. $A2\times2\times2$ k mash was used with the plane-wave cutoff energy (E_{cut}) of 400 eV, in order to confirm the convergence with respect to E_{cut}, the formation energies of the defect structure were also calculated at E_{cut} =530 eV. The resulted formation energies at E_{cut}=400 eV were then found to converge within 0.1 eV as compared to the higher cut-off energy.

B. Defect-formation energies

The defect-formation energies in $LaAlO_3$ can be calculated from the total energy of the supercell with defects, following the approach described in previous reports.[26,27] The formation energies of charged defects will depend on the atomic chemical potentials and also vary with the electron chemical potential such as the Fermi energy. For a supercell containing defect α with charge state q, the formation energy is given by

$$\Omega_f(\alpha,q) = E_{sc}(\alpha,q) - \sum_i n_i\mu_i + q(\mu_e + E_{\mathrm{VBM}}) \qquad (1)$$

In this expression, $E_{sc}(\alpha,q)$ represents the total energy of the supercell containing charged defect α, n_i is the number of La, Al, and O atoms in the supercell, respectively, and μ_i is their corresponding atomic chemical potentials. The q is the charge of defect and it varies from neutral to fully ionized states. At T=0, the entropy contribution is neglected, the Fermi energy μ_e is measured from the top of the valence band and varies from zero to the value of band gap. E_{VBM} is the one-electron energy of the valence-band maximum (VBM), it is expected that the E_{VBM} of a defect containing supercell is different from that of the perfect supercell due to the band-gap distortion caused by the defect.

In order to obtain the formation energy of a charged defect, it is necessary to determine E_{VBM} of the defective supercell and to line up the band structures with the perfect supercell. It is assumed that the potentials of atoms in the perfect supercell are similar to those far from a defect in the defective supercell. Then the shift of the VBM in a defective supercell can be obtained by using a macroscopic averaging technique,[28,29] which calculated the average electrostatic potential difference between the defect containing supercell and the defect-free supercell. In the finite-size supercell calculation, these treatments can compensate the error caused by Coulomb interaction between the charged defects and the background image charge.[30]

The defect-formation energies in $LaAlO_3$ are a function of the component chemical potentials. However, the chemical potential of the atomic species cannot be obtained directly. In the thermodynamic equilibrium, there are some thermodynamic limits for the chemical potentials

$$\mu_{\mathrm{La}} + \mu_{\mathrm{Al}} + 3\mu_{\mathrm{O}} = \mu_{\mathrm{LaAlO_3}} \qquad (2)$$

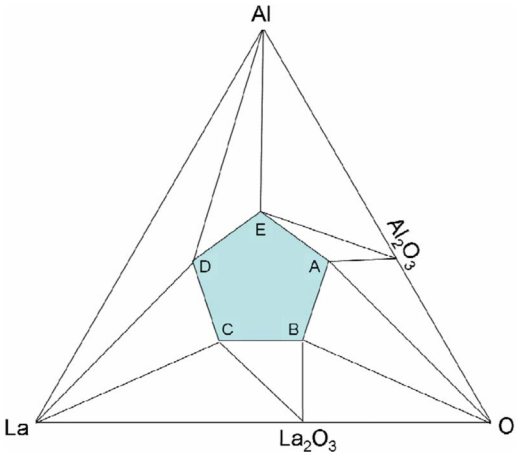

FIG. 2. (Color online) The schematic phase diagram of the La-O-Al ternary system.

$$\mu_{\mathrm{La}} \le 0, \quad \mu_{\mathrm{Al}} \le 0, \quad \mu_{\mathrm{O}} \le 0, \qquad (3)$$

where $\mu_{\mathrm{LaAlO_3}}$ is the generalized free formation energy per f.u. of the perfect $LaAlO_3$. These conditions are applied to the ternary $LaAlO_3$ system and allow determining the chemical potential from the various equilibrium conditions. Similar to the phase diagram of SrTiO3,[27] Fig. 2 shows the phase diagram of the ternary La-Al-O system, which is derived from the combination of the chemical potentials of Al, Al_2O_3, La, La_2O_3, and O_2. The vertices of the triangle correspond to three dominant component chemical potentials and the compounds are placed on the edge according to their stoichiometric proportion. Points A–E denoted the five possible chemical-potential combinations and the intersections of these five points define the thermodynamically equilibrium region of the ternary system under different chemical potentials. At points A and B, the chemical potentials for O are similar to a strongly oxidation environment like those $LaAlO_3$ sample grown in an O_2 rich state. On the contrary, at point D the system is in a strongly reducing environment. Under the assumption that $LaAlO_3$ is always stable, the atomic chemical potentials for La, Al, and O are constrained by the following equilibrium equations:

$$\text{Point A:} 2\mu_{\mathrm{Al}} + 3\mu_{\mathrm{O}} = \mu_{\mathrm{Al_2O_3}}, \quad \mu_{\mathrm{O}} = \mu_{\mathrm{O}(bulk)}, \qquad (4)$$

$$\text{Point B:} 2\mu_{\mathrm{La}} + 3\mu_{\mathrm{O}} = \mu_{\mathrm{La_2O_3}}, \quad \mu_{\mathrm{O}} = \mu_{\mathrm{O}(bulk)}, \qquad (5)$$

$$\text{Point C:} 2\mu_{\mathrm{La}} + 3\mu_{\mathrm{O}} = \mu_{\mathrm{La_2O_3}}, \quad \mu_{\mathrm{La}} = \mu_{\mathrm{La}(bulk)}, \qquad (6)$$

$$\text{Point D:} \mu_{\mathrm{Al}} = \mu_{\mathrm{Al}(bulk)}, \quad \mu_{\mathrm{La}} = \mu_{\mathrm{La}(bulk)}, \qquad (7)$$

$$\text{Point E:} 2\mu_{\mathrm{Al}} + 3\mu_{\mathrm{O}} = \mu_{\mathrm{Al_2O_3}}, \quad \mu_{\mathrm{Al}} = \mu_{\mathrm{Al}(bulk)}. \qquad (8)$$

The chemical potential of O_2 was calculated from the total energy of the O_2 molecule using a cubic box with length of 10 Å. In the above equilibrium states, the bulk materials of La (FCC), Al (FCC), La_2O_3 (P-3M1), and Al_2O_3 (R-3CH) are calculated to determine the atomic chemical potentials in their phase. The calculated and experimental enthalpies of

TABLE II. Calculated and experimental enthalpies of formation for the perfect $LaAlO_3$, La_2O_3, and Al_2O_3.

	Enthalpy of formation (eV/atom)	
Materials	Calculated	Experimental
$LaAlO_3$	−3.597	−3.45[a]
La_2O_3	−3.713	−3.71[b]
Al_2O_3	−3.303	−3.47[c]

[a]Reference 31.
[b]Reference 32.
[c]Reference 33.

formation are given in Table II, where spin-polarization is taken into account in our calculations. It can be seen that the calculated enthalpies of formation are in close agreement with the experimental values.[31–33]

In electronic devices, the positions of the defect levels with respect to the bottom of the conduction band of $LaAlO_3$ and to other electron sources such as Si are useful. To achieve that, we need to calculate the electron affinity, which is defined as the energy gained when a free electron from the bottom of the conduction band is trapped at the defect. The electron affinity with charge q is computed by comparing the total energies of the initial and final states with different electrons. In our large supercell calculation, the GGA calculation gave a band gap of 3.63 eV. The difference κ (1.97 eV) in the band gap between the theoretical and the experimental value is the main source of error in the defect-level alignment.[34] Under the assumption that the underestimation of the band gap is due to the low position of the bottom of the conduction band,[35] the difference κ between the calculated and experimental energy band gap are used to correct the electron affinity.

$$\chi_e(\alpha,q) = E_{sc}(\alpha,q) + E(\mathrm{LaAlO_3},-) - E_{sc}(\alpha,q-1) - E(\mathrm{LaAlO_3},0) + \kappa, \quad (9)$$

where $E(\mathrm{LaAlO_3},-)$ and $E(\mathrm{LaAlO_3},0)$ are the calculated energies of the perfect supercell with charge −1 and 0, respectively. Similarly we can define the hole affinity of the defect, the energy gained when a free hole from the top of the valence band is trapped to the defect

$$\chi_h(\alpha,q) = E_{sc}(\alpha,q) + E(\mathrm{LaAlO_3},+) - E_{sc}(\alpha,q+1) - E(\mathrm{LaAlO_3},0) \quad (10)$$

Using these definitions, the equation $\chi_e(\alpha,q)+\chi_h(\alpha,q) = E_g(\mathrm{Exp})$ is satisfied. Now the theoretical results are in scale with experiment and thus we can use the experimental value of the band offset with Si to align the various defect levels.

III. RESULTS AND DISCUSSION

A. System size and structure relaxation

The formation energies of a variety of neutral and charged intrinsic defects are studied by using supercell calculations.

TABLE III. Defect-formation energies of various isolated defects in different supercell sizes (20, 40, 90, and 135 atoms). The chemical potential is fixed at point A (oxidizing conditions) in the calculations.

	Supercell size and formation energies (eV)			
Defect	20	40	90	135
O_i^0	6.409	4.601	4.437	4.404
O_i^{1-}	6.620	4.837	4.471	4.464
O_i^{2-}	3.621	4.696	4.431	4.392
V_O^0	6.727	6.464	6.408	6.545
V_O^{1+}	6.593	6.544	6.562	6.475
V_O^{2+}	3.141	1.805	0.996	1.084
Al_i^0	22.552	17.087	16.608	16.545
Al_i^{1+}	22.587	16.345	16.486	16.271
Al_i^{2+}	22.938	16.195	16.578	16.105
Al_i^{3+}	14.818	8.077	7.038	7.203
V_{Al}^0	3.168	3.931	3.814	3.674
V_{Al}^{1-}	4.234	4.019	3.848	3.704
V_{Al}^{2-}	3.953	3.823	3.799	3.759
V_{Al}^{3-}	4.133	3.915	3.812	3.803
La_i^0	32.299	23.760	22.444	22.773
La_i^{1+}	31.741	24.194	22.062	22.332
La_i^{2+}	31.383	23.984	21.886	21.874
La_i^{3+}	30.779	16.839	13.899	13.779
V_{La}^0	2.262	1.997	1.887	1.798
V_{La}^{1-}	2.402	2.150	1.927	1.828
V_{La}^{2-}	2.081	2.167	2.008	1.875
V_{La}^{3-}	1.045	2.249	1.940	1.915
La_{Al}	9.662	8.063	7.964	7.680
Al_{La}	5.774	5.820	5.222	5.831
O_{FP}	14.368	12.751	12.301	12.10
Al_{FP}	25.191	24.47	24.645	24.55
$V_{Al}^{3-}+V_{La}^{3-}+3V_O^{2+}$		5.210		5.00

In order to derive the formation energy in the dilute limit, the effects of supercell size convergence on the formation energy are studied, as displayed in Table III. Results for different supercell sizes (20, 40, 90, and 135 atoms) are shown, with the reference chemical potential fixed at point A as shown in Fig. 2. The oxidizing conditions at point A are suitable to simulate the thin-film deposition on the silicon substrate and the following thermal processes in the CMOS technique. The lattice distortion induced by the different supercell is significant, the lattice constants vary from 2% to 0.8% in the $1\times2\times2$ supercell (20 atoms) and the $3\times3\times3$ supercell (135 atoms), respectively. From Table III, it can be seen that the lattice distortions have a minor influence on the formation energies when the system is larger than $3\times3\times2$ supercell (90 atoms). It is noted that the formation energy of the neutral defects began to show convergence at the $2\times2\times2$ supercell while the high q charged defects such as V_O^{2+}, V_{La}^{3-}, La_i^{3+}, and Al_i^{3+} require a larger $3\times3\times2$ supercell (90 atoms)

TABLE IV. The distances of the neighboring ions from a vacancy before and after the structural relaxation.

	Distance (Å) (change in percentage)		
Vacancies	First NN	Second NN	Third NN
La (bulk)	2.71 (O^*12)	3.32 (Al^*8)	3.83 (La^*6)
V_{La}^{0}	2.78 (2.58%)	3.23 (–2.71%)	3. 80 (–0.78%)
V_{La}^{1-}	2.79 (2.95%)	3.24 (–2.41%)	3.80 (–0.78%)
V_{La}^{2-}	2.79 (2.95%)	3.24 (–2.41%)	3.81 (–0.52%)
V_{La}^{3-}	2.80 (3.32%)	3.25 (–2.11%)	3.81 (–0.52%)
Al (bulk)	1.91 (O^*6)	3.32 (La^*8)	3.83 (Al^*6)
V_{Al}^{0}	2.00 (4.71%)	3.12 (–6.02%)	3.84 (0.26%)
V_{Al}^{1-}	2.01 (5.24%)	3.11 (–6.33%)	3.85 (0.52%)
V_{Al}^{2-}	2.02 (5.76%)	3.10 (–6.63%)	3.85 (0.52%)
V_{Al}^{3-}	2.03 (6.28%)	3. 09 (–6.93%)	3.86 (0.78%)
O (bulk)	1.91 (Al^*2)	2.71 (O^*8, La^*4)	3.83 (O^*6)
V_{O}^{0}	1.92 (0.53%)	2.70 (–0.37%), 2.71 (0.00%)	3.82 (–0.26%)
V_{O}^{1+}	1.97 (3.17%)	2.62 (–3.36%), 2.72 (0.37%)	3.81 (–0.53%)
V_{O}^{2+}	2.01 (5.29%)	2.54 (–6.34%), 2.75 (1.49%)	3.78 (–1.32%)

to converge. Certainly, the $3\times3\times2$ (90 atoms) and $3\times3\times3$ (120 atoms) supercell produce similar results for various types of defects. Therefore, this minor difference in formation energies also indicates that the interaction between a defect and its images can be neglected in the large $3\times3\times3$ supercell. In the following calculations, the structure relaxation and defect-formation energies are based on the $3\times3\times3$ supercell.

The formation of defects will cause structural distortions around the defects. Table IV lists the distances from a vacancy to the neighboring ions before and after structural relaxation of the supercell. The first nearest-neighboring (NN) ions about the vacancy move outward, irrespective of the charge state. In contrast, the second NN ions exhibit more inward relaxation, except for the case of V_O. The V_O has two different second NN ion species (La and O), which occupy the equivalent coordinates. As a result of the V_O relaxation, La ions tend to be pushed, while O ions are pulled toward the vacancy.

These ions relaxations can be explained from the balance of the electrostatic force. The outward relaxation of the first NN is a result of the missing chemical bonds, which attract the removed cations (anions) and the surrounding anions (cations). The inward movement of the second NN ions can be understood since the electrostatic repulsions of the cations (anions) and the removed cations (anions) are reduced by the introduction of a vacancy. For all vacancy species, with the increase in the charge state, the amplitude of the relaxation around the vacancy becomes larger. It is clear that a higher charged vacancy will have a stronger electrostatic reaction with the surrounding ions.

Moreover, the V_{Al} causes a larger atomic relaxation (about twice as compared to the V_{La}) and is more sensitive to the charged state. The different relaxation behaviors for cation vacancies (V_{La} and V_{Al}) are due to the different strength of the covalent interaction between La-O and Al-O atoms. The Al-O atoms show a larger *sp* states hybridization in the DOS plotted in Fig. 1, indicating a stronger covalent bonding as compared with La-O atoms. Further investigations on the Mulliken charge and bond population[20,36] have shown that the overlap electron population between Al-O bonding is 0.39 e, twice as high as that of the La-O bonding (0.18 e). This charge transfer played an important role in stabilizing the structure with a large lattice relaxation. The strong Al-O bonding was broken after the introduction of cation vacancy thus the O atoms about V_{Al} have a larger outward relaxation than those about V_{La}. For the second NN ions about V_{Al}, with a force analysis, it is found that the more inward relaxation of La atoms is the result of the looser La-O constrain. It is noted that, in the third NN ions, the distances of atoms did not change significantly, indicating the minor influence from the vacancy. The cutoff radius of the third NN selected here is sufficient to describe the structural relaxations around vacancies.

B. Formation energy

Figure 3 shows the formation energies of various defects along the vertices ($A\rightarrow B\rightarrow C\rightarrow D\rightarrow E$) defined in Fig. 2. It can be seen from Fig. 3 that the neutral vacancies and interstitials vary their formation energies in different chemical environment. The O vacancy V_O is a stable defect under reducing conditions. And the V_O keeps the lowest formation energy over a broad range of chemical potentials, a result that is consistent with many experimental findings.[37,38] Under oxidizing conditions, the vacancies of La and Al exhibit

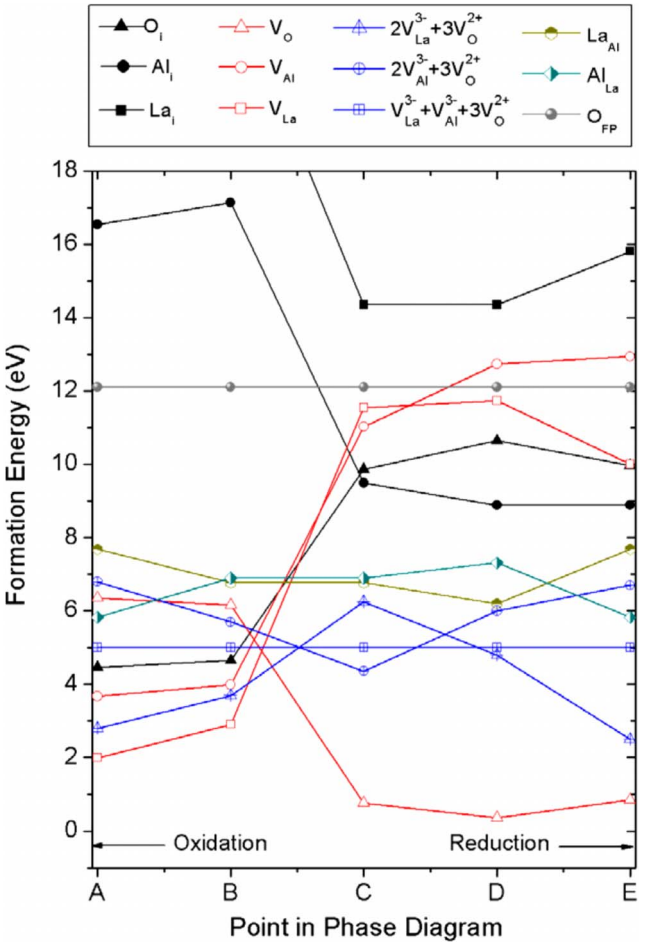

FIG. 3. (Color online) Formation energies for isolated intrinsic defects in $LaAlO_3$ at each equilibrium points of La-O-Al ternary phase diagram.

their lowest formation energy, which suggest that the metal vacancies are easily formed under O_2-rich atmosphere. In contrast, the formation energies of cation interstitials are found to be relatively high compared to vacancies. The microscopic origin of that may arise from the large electrostatic repulsions suffered by the interstitials in the surrounding environment.

The O Frenkel pair-formation energies in Fig. 3 remain constant, irrespective of the component chemical potentials, because the whole system of $LaAlO_3$ is still stoichiometric even after the Frenkel pair formation. The same reason is suitable for the full Schottky defect $V_{Al}^{3-}+V_{La}^{3-}+3V_O^{2+}$, which has formation energy of 5.0 eV. The formation energy of the O Frenkel pair is almost the sum of a separate vacancy and interstitial, which may serve as an indication of weak interaction between the O interstitial and vacancy. Among the antisite defects, the Al_{La} antisite has the lowest formation energy at both reducing and oxidizing conditions. As compared to the O Frenkel pair, the partial Schottky of $2V_{Al}^{3-}+3V_O^{2+}$ and $2V_{La}^{3-}+3V_O^{2+}$ exhibit smaller energies at all equilibrium points.

Besides neutral defects in the $LaAlO_3$ bulk samples, charge defects can also generate due to the growth, doping type, and thermal processes. Therefore, we study the formation energies of charged defects as a function of the electronic chemical potential (Fermi levels) μ_e shown in Fig. 4. The chemical environment at points A and E (in Fig. 2) are focused in Figs. 4(a) and 4(b), respectively. The formation energy of a defect with a particular charged state is only shown when the charge state has the lowest energy. So the slope of a line corresponds to a charge defect state and the change in slope indicates a transition between charged states. In Fig. 4(a), corresponding to the oxidizing conditions, the V_O^{2+} is the dominant defect above the top of VBM, but its energy increase as the Fermi level μ_e increase. At the bottom of the conduction band, the neutral V_O^0 become stable. The cation vacancies prefer neutral states about the VBM and negatively charged states are stable as the μ_e increase. Thus V_{La}^{3-} and V_{Al}^{3-} dominate in a wide range, especially near the bottom of the conduction band. While for O interstitial, only the paired negative charged O_i^{2-} is preferred at the whole range of the electron chemical potential. As can be seen from Fig. 4(b), at point E under reducing conditions, the formation energies for all the charged vacancies and interstitials have a similar trend as that in Fig. 4(a). The main difference is that the formation energies of V_{La}^{3-} and V_{Al}^{3-} further increase, whereas the formation energy for V_O^{2+} decreases. Decreasing the O partial pressure will stabilize the V_O^{2+} defect at lower Fermi level.

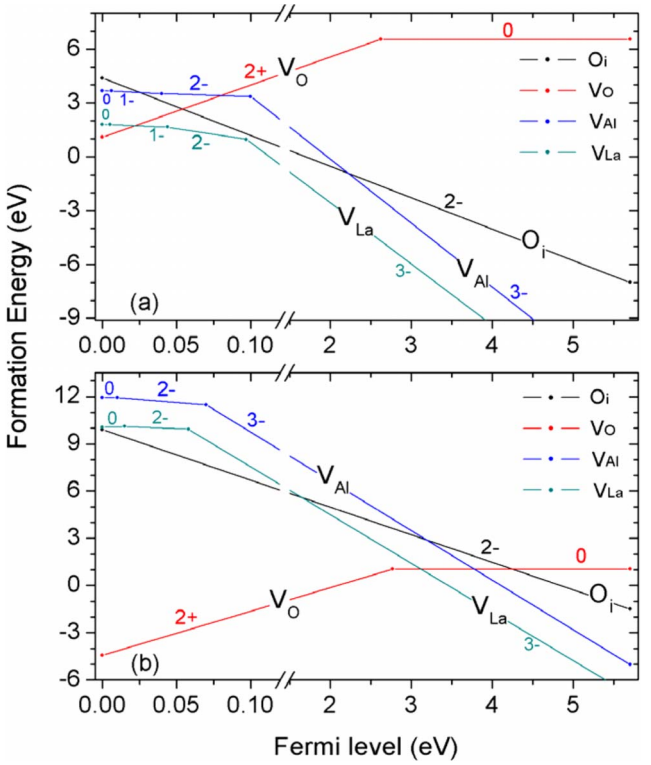

FIG. 4. (Color online) Formation energies as a function of the electronic chemical potential. (a) The atomic chemical potentials correspond to the values of equilibrium point A and (b) E. Only the charged states with the lowest formation energy are depicted.

C. Model processes

Assuming that the distributions of the defects in different charged states are known, we can use the defect reaction

TABLE V. Calculated defect reactions, the associated energies are obtained from the formation energies of isolated defects in the $3\times3\times3$ supercell (135 atoms).

No.	Reaction	Energy (eV)
1	$O_i^0+O_i^{2-}\rightarrow 2O_i^-$	−0.132
2	$O_i^0+V_O^0\rightarrow O_i^-+V_O^+$	0.011
3	$O_i^-+V_O^+\rightarrow O_i^{2-}+V_O^{2+}$	5.463
4	$O_i^0+V_O^0\rightarrow O_i^{2-}+V_O^{2+}$	5.474
5	$V_O^0+V_O^{2+}\rightarrow 2V_O^+$	−5.321
6	$Al_i^0+Al_i^{2+}\rightarrow 2Al_i^+$	0.107
7	$Al_i^0+V_{Al}^0\rightarrow Al_i^++V_{Al}^-$	0.244
8	$Al_i^0+V_{Al}^0\rightarrow Al_i^{2+}+V_{Al}^{2-}$	1.339
9	$Al_i^0+V_{Al}^0\rightarrow Al_i^{3+}+V_{Al}^{3-}$	9.214
10	$V_{Al}^0+V_{Al}^{2-}\rightarrow 2V_{Al}^-$	0.025
11	$La_i^0+La_i^{2+}\rightarrow 2La_i^+$	−0.017
12	$La_i^0+V_{La}^0\rightarrow La_i^++V_{La}^-$	0.411
13	$La_i^0+V_{La}^0\rightarrow La_i^{2+}+V_{La}^{2-}$	0.822
14	$La_i^0+V_{La}^0\rightarrow La_i^{3+}+V_{La}^{3-}$	8.878
15	$V_{La}^0+V_{La}^{2-}\rightarrow 2V_{La}^-$	0.018

analysis to predict which kind of defect combinations will be energetically favorable. Table V shows various reactions and their energies, which are obtained from the formation energies of isolated charged interstitials and vacancies under oxidizing conditions. A positive value of the reaction energy indicates that the reaction is energetically favorable.

The O interstitial will forms a "dumbbell" or a "balance-shaped" structure with the surrounding O ions in the lattice, depending on the initial position of the interstitial atom. Reaction 1 in Table V shows that, similar to the calculation of zirconia,[39,40] the O interstitials reaction predicts an Anderson's "negative −U" behavior,[41] namely, that two isolated O_i^- species will decay into a O_i^{2-} and a neutral O_i^0. Since the net electron-electron coupling is attractive in O_i^{2-} and this reaction is energetically favorable. The same is true for the O vacancies in reaction 5 but with a larger energy gain: two isolated V_O^+ centers are not stable, they would decay into a paired charged and a neutral O vacancy. As mentioned in the structural relaxation, the neighboring ions move slightly outward about an O vacancy, and thus introduce a similar distortion as an O interstitial, all having the negative −U behavior. This also means that in $LaAlO_3$ both the O vacancy and interstitial would prefer to stay in diamagnetic states, which would be difficult to detect by using paramagnetic resonance measurement. For the O Frenkel pairs in reaction 2–4, the neutral interstitial and vacancy did not have a strong interaction in the relaxed structure. The energy of the charged pairs is slightly different. The separated pair of doubly charged $O_i^{2-}+V_O^{2+}$ is energetically favorable since its associated formation energy is 5.463 eV lower than the singly charged pair $O_i^-+V_O^+$, and 5.474 eV lower than a pair of neutral defect. The difference in the charged pair-formation energies indicates a tendency toward charge transfer between the O vacancies and interstitials.

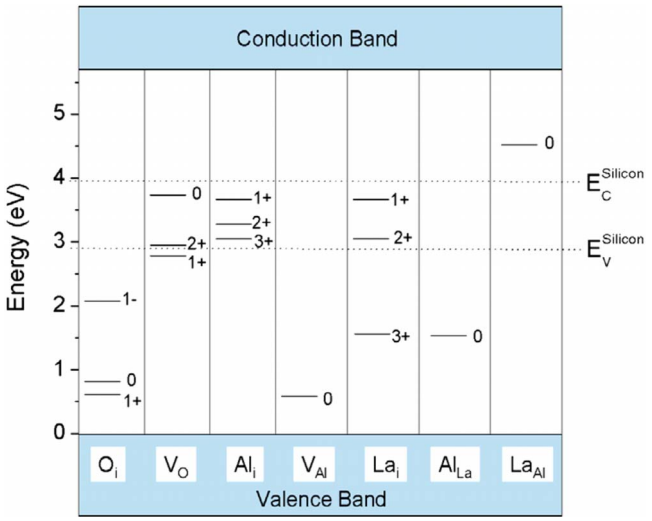

FIG. 5. (Color online) Energy-level diagram showing the electron affinities for various defects in $LaAlO_3$, and the reference of the conduction and valence-band edges of Silicon.

Besides the O defect reactions, the cation defect reactions are also discussed. From reaction 6 in Table V, the singly charged Al interstitial is most favorable, but the corresponding energy gain is small and will change with the external temperature. Again, there is also a negative −U behavior for the charged vacancy defect in reaction 11 $La_i^0+La_i^{2+}\rightarrow 2La_i^+$, when two La_i^+ decay into neutral and paired charged Al vacancy, it will release energy of 0.017 eV. For the rest cation Frenkel pair reaction, the charge transfer between the vacancy and interstitial is favorable. It is noted that the formation energy of the triple charged Al Frenkel pair is 9.214 eV lower than the neutral Al Frenkel pair, showing the strong ionic character of these defects.

D. Electron trapping

The presence of intrinsic point defects in $LaAlO_3$ will affect the performance of this material as an alternative gate dielectric. Therefore it is important to simulate the activity of defect states with respect to the $LaAlO_3$ and silicon conduction bands in the CMOS devices, where the electrons can tunnel from the thin oxide potentials into the defect states. The large electron affinities of the interstitial species and charged vacancies may serve as traps for electrons generated from the valence band of $LaAlO_3$. According to Eq. (9), the calculated electron affinities of these defects are shown in a schematic energy diagram (Fig. 5) together with the reference of the silicon valence and conduction-band edge at the $Si/LaAlO_3$ interface. The alignment of the defect levels with the valence-band edges will determine whether these defects can play a role in the conductivity.

Recent x-ray photoelectron spectroscopy measurement showed that crystalline $LaAlO_3$ forms an adequate barrier for both electrons and holes, the valence-band offset (VBO) between $LaAlO_3$ films and Si is measured to be 2.86 eV.[4] Counting from the top of the valence band of $LaAlO_3$, we used the experimental VBO at the $Si/LaAlO_3$ interface and

the band gap of silicon to estimate the tunneling energy of electrons with respect to the defect states. Figure 5 shows the defect levels of various intrinsic defects in cubic $LaAlO_3$. The oxygen interstitials O_i, Al_{La} antisite, and the Al vacancy V_{Al} will act as acceptors and can trap electrons injected from the top of the valence band of $LaAlO_3$. The donor levels for La_{Al} antisite lies above the silicon conduction-band minimum (CBM) and would probably produce electrons into the silicon. The deep level of V_O and the cation interstitials (Al_i and La_i) could be problematic since their positions lie in the silicon energy gap and may serve as pin in the band gap. That will facilitate the electron tunneling from the silicon valence band and give rise to a large conductivity, especially for V_O^{2+}, which has the lowest formation energy near the $LaAlO_3$ VBM. Similar to the situation of HfO_2, the presence of reducing conditions and the adjacent metal gate will make a large concentration of V_O occur in the gate oxides. The deep defect level of neutral V_O, would probably resonate with the bottom of the silicon conduction band, and form the electron-trapping site to impair the barrier potential, resulting in a large-tunneling-leakage current. These results are consistent with experimental observations.[42]

The energetic studies can only predict the energy gain during these processes at zero temperature. However, the real possibility of such processes still needs to know the kinetics of the defect electron trapping at finite temperature, which requires a further study regarding the scattering cross sections for electron trapping on these defects. It is also noted that the dielectric thin film used in CMOS is just several atomic monolayer, where the size effect, quantum tunneling, large surface proportion, and the substrate strain become dominant. These combinations of factors will have pivotal influences on its electrical and elastic properties but not so much on the formation energy. Since the thin film also has the same defect structures as in the bulk material, the energy of defects in bulk material can shed light on the thin-film system. The defect structures in thin film and their influence on the electronic-transport properties will be discussed in the future works.

IV. CONCLUSIONS

The structural relaxations and formation energy of various intrinsic defects in cubic $LaAlO_3$ have been investigated by first-principles plane-wave-based pseudopotential calculations. In summary, our analysis of this work yields the following conclusions: (1) for all vacancy species, irrespective the charge state, the relaxation of the first NN ions exhibits an outward trend. In contrast, the second NN ions show an inward movement except for V_O, which pulls the O and pushes the La ions. Moreover, it is found that the ions about V_{Al} exhibit larger atomic relaxation as compared to those about V_{La}. (2) Under reducing conditions, the O vacancy is the most stable defect in $LaAlO_3$ and V_O^{2+} is the dominant defect when the Fermi level is close to the VBM. In contrast, under oxidizing conditions, negative cation vacancies such as V_{La}^{3-} and V_{Al}^{3-} become dominant as the Fermi level increases. There is a strong negative –U behavior in the O vacancy reactions, indicating strong tendency for two isolated V_O^+ species to decay into V_O^{2+} and V_O^0. (3) The intrinsic defect levels are aligned with respect to the $LaAlO_3$ and silicon conduction bands. The O_i interstitial, Al_{La} antisite, and the V_{Al} vacancy will act as acceptor for electrons, and V_O vacancy, Al_i, and La_i interstitials will give rise to a large conductivity due to their deep defect levels lying in the middle of the silicon band gap. In particular, the paired charged V_O is identified as the key defect, which is conjectured to play an important role in leakage currents, have been verified to indeed have the lowest formation energy in reducing conditions.

ACKNOWLEDGMENTS

This work was supported by the National Natural Science Foundation of China (NSFC) (Grants No. 10572155, No. 10902118, No. 10732100, No. 10831160504) and the Guangdong Science and Technology Bureau (Grant No. 2006A11001002). The authors thank Q. K. Li and D. Huang for stimulating discussions.

*wangbiao@mail.sysu.edu.cn

[1] The International Technology Roadmap for Semiconductors, 2008, http://public/itrs.net
[2] D. A. Muller, T. Sorsch, S. Moccio, F. H. Baumann, K. Evans-Lutterodt, and G. Timp, Nature (London) **399**, 758 (1999).
[3] S. G. Lim, S. Kriventsov, T. N. Jackson, J. H. Haeni, D. G. Schlom, A. M. Balbashov, R. Uecker, P. Reiche, J. L. Freeouf, and G. Lucovsky, J. Appl. Phys. **91**, 4500 (2002).
[4] Y. Y. Mi, Z. Yu, S. J. Wang, P. C. Lim, Y. L. Foo, A. C. H. Huan, and C. K. Ong, Appl. Phys. Lett. **90**, 181925 (2007).
[5] B. E. Park and H. Ishiwara, Appl. Phys. Lett. **82**, 1197 (2003).
[6] W. Xiang, H. Lü, L. Yan, H. Guo, L. Liu, Y. Zhou, G. Yang, J. Jiang, H. Cheng, and Z. Chen, J. Appl. Phys. **93**, 533 (2006).
[7] D. O. Klenov, D. G. Schlom, H. Li, and S. Stemmer, Jpn. J. Appl. Phys., Part 2 **44**, L617 (2005).
[8] M. Suzuki, M. Tomita, T. Yamaguchi, and N. Fukushima, Tech. Dig. - Int. Electron Devices Meet. **2005**, 445.
[9] A. Ohtomo and H. Y. Hwang, Nature (London) **427**, 423 (2004); Nature (London) **441**, 120 (2006).
[10] M. Basletic, J. L. Maurice, C. Carrétéro, G. Herranz, O. Copie, M. Bibes, É. Jacquet, K. Bouzehouane, S. Fusil, and A. Barthélémy, Nature Mater. **7**, 621 (2008).
[11] C. J. Först, K. Schwarz, and P. E. Blöchl, Phys. Rev. Lett. **95**, 137602 (2005).
[12] Y. F. Dong, Y. Y. Mi, Y. P. Feng, A. C. H. Huan, and S. J. Wang, Appl. Phys. Lett. **89**, 122115 (2006).
[13] K. Xiong, J. Robertson, and S. J. Clark, Appl. Phys. Lett. **89**, 022907 (2006).
[14] G. Kresse and J. Furthmuller, Phys. Rev. B **54**, 11169 (1996).
[15] P. E. Blöchl, Phys. Rev. B **50**, 17953 (1994).
[16] G. Kresse and D. Joubert, Phys. Rev. B **59**, 1758 (1999).
[17] J. P. Perdew, K. Burke, and M. Ernzerhof, Phys. Rev. Lett. **77**,

3865 (1996).
[18] A. A. Knizhnik, I. M. Iskandarova, A. A. Bagatur'yants, B. V. Potapkin, L. R. C. Fonseca, and A. Korkin, Phys. Rev. B **72**, 235329 (2005).
[19] X. Gonze, G.-M. Rignanese, M. Verstraete, J.-M. Beuken, Y. Pouillon, R. Caracas, F. Jollet, M. Torrent, G. Zerah, M. Mikami, Ph. Ghosez, M. Veithen, J.-Y. Raty, V. Olevano, F. Bruneval, L. Reining, R. Godby, G. Onida, D. R. Hamann, and D. C. Allan, Z. Kristallogr. **220**, 558 (2005).
[20] X. Luo and B. Wang, J. Appl. Phys. **104**, 053503 (2008).
[21] E. Cicerrella, J. L. Freeouf, L. F. Edge, D. G. Schlom, T. Heeg, J. Schubert, and S. A. Chambers, J. Vac. Sci. Technol. A **23**, 1676 (2005).
[22] C. J. Howard, B. J. Kennedy, and B. C. Chakoumakos, J. Phys.: Condens. Matter **12**, 349 (2000).
[23] P. Bouvier and J. Kreisel, J. Phys.: Condens. Matter **14**, 3981 (2002).
[24] P. Delugas, V. Fiorentini, and A. Filippetti, Phys. Rev. B **71**, 134302 (2005).
[25] G. Makov and M. C. Payne, Phys. Rev. B **51**, 4014 (1995).
[26] S. B. Zhang and J. E. Northrup, Phys. Rev. Lett. **67**, 2339 (1991).
[27] T. Tanaka, K. Matsunaga, Y. Ikuhara, and T. Yamamoto, Phys. Rev. B **68**, 205213 (2003).
[28] A. Baldereschi, S. Baroni, and R. Resta, Phys. Rev. Lett. **61**, 734 (1988).
[29] M. Peressi, N. Binggeli, and A. Baldereschi, J. Phys. D **31**, 1273 (1998).
[30] R. Astala and P. D. Bristowe, Model. Simul. Mater. Sci. Eng. **9**, 415 (2001).
[31] W. Schnelle, R. Fischer, and E. Gmelin, J. Phys. D **34**, 846 (2001).
[32] E. H. P. Cordfunke and R. J. M. Konings, Thermochim. Acta **375**, 65 (2001).
[33] *NIST Chemistry WebBook*, in NIST Standard Reference Database No. 69, edited by W. G. Mallard and P. J. Linstrom (National Institute of Standards and Technology, Gaithersburg, MD, 2008).
[34] J. M. Pruneda and E. Artacho, Phys. Rev. B **71**, 094113 (2005).
[35] A. S. Foster, F. L. Gejo, A. L. Shluger, and R. M. Nieminen, Phys. Rev. B **65**, 174117 (2002).
[36] X. Luo and B. Wang, J. Appl. Phys. **104**, 073518 (2008).
[37] W. Siemons, G. Koster, H. Yamamoto, W. A. Harrison, G. Lucovsky, T. H. Geballe, D. H. A. Blank, and M. R. Beasley, Phys. Rev. Lett. **98**, 196802 (2007).
[38] A. Kalabukhov, R. Gunnarsson, J. Börjesson, E. Olsson, T. Claeson, and D. Winkler, Phys. Rev. B **75**, 121404 (2007).
[39] A. S. Foster, V. B. Sulimov, F. L. Gejo, A. L. Shluger, and R. M. Nieminen, Phys. Rev. B **64**, 224108 (2001).
[40] J. X. Zheng, G. Ceder, T. Maxisch, W. K. Chim, and W. K. Choi, Phys. Rev. B **75**, 104112 (2007).
[41] P. W. Anderson, Phys. Rev. Lett. **34**, 953 (1975).
[42] E. P. Gusev, V. Narayanan, S. Zafar, C. Cabral, E. Cartier, N. Bojarczuk, A. Callegari, R. Carruthers, M. Chudzik, C. Demic, E. Duch, P. Jamison, P. Kozlowski, D. Latulipe, K. Maitra, F. R. Mcfeely, J. Newbury, V. Paruchuri, and M. SteenTech. Dig. - Int. Electron Devices Meet. **2004**, 729.